AGU PUBLICATIONS

Geophysical Research Letters

RESEARCH LETTER
10.1002/2015GL063413

Key Points:
- The mean and variance of catchment elevation distributions impact SWE loss
- Midelevation distributions with small variance are most sensitive to SWE loss
- Landscape patterns of simulated SWE loss are nonlinear and elevation dependent

Supporting Information:
- Text S1, Figures S1–S6, and Tables S1–S3

Correspondence to:
C. J. Tennant,
tennchri@isu.edu

Citation:
Tennant, C. J., B. T. Crosby, S. E. Godsey, R. W. VanKirk, and D. W. R. Derryberry (2015), A simple framework for assessing the sensitivity of mountain watersheds to warming-driven snowpack loss, *Geophys. Res. Lett.*, *42*, doi:10.1002/2015GL063413.

Received 9 FEB 2015
Accepted 3 MAR 2015
Accepted article online 7 MAR 2015

A simple framework for assessing the sensitivity of mountain watersheds to warming-driven snowpack loss

Christopher J. Tennant[1], Benjamin T. Crosby[1], Sarah E. Godsey[1], Robert W. VanKirk[2,3], and DeWayne R. Derryberry[4]

[1]Department of Geosciences, Idaho State University, Pocatello, Idaho, USA, [2]Henry's Fork Foundation, Ashton, Idaho, USA, [3]Department of Mathematics, Humboldt State University, Arcata, California, USA, [4]Department of Mathematics, Idaho State University, Pocatello, Idaho, USA

Abstract The common observation that snowpack increases with elevation suggests that a catchment's elevation distribution should be a robust indicator of its potential to store snow and its sensitivity to snowpack loss. To capture a wide range of potential elevation-based responses, we used Monte Carlo methods to simulate 20,000 watershed elevation distributions. We applied a simple function relating warming, elevation, and snowpack to explore snowpack losses from the simulated elevation distributions. Regression analyses demonstrate that snowpack loss is best described by three parameters that identify the central tendency, variance, and shape of each catchment's elevation distribution. Equal amounts of snowpack loss can occur even when catchments are centered within different elevation zones; this stresses the value of also measuring the variance and shape of elevation distributions. Responses of the simulated elevation distributions to warming are nonlinear and emphasize that the sensitivity of mountain forests to snowpack loss will likely be watershed dependent.

1. Introduction

Throughout the world, communities living in dry low-elevation valleys depend on water from high-elevation snowpack. The timing and amount of water release from snowpack sets the pace and potential of human activities such as irrigation, power generation, and availability of municipal water supply [*Clark*, 2010]. Recent studies have documented a reduction in the proportion of precipitation falling as snow [*Knowles et al.,* 2006], widespread decreases in snow water equivalent (SWE) [*Mote et al.,* 2005], and earlier snowmelt from mountain regions [*Stewart*, 2009]. Many of these changes are linked to increases in the elevation of the freezing level [*Abatzoglou*, 2011] and accelerated warming at high elevations [*Rangwala and Miller,* 2012]. Warming and changes in snow accumulation and melt have important implications for the spatial distribution of plant communities [*Ford et al.,* 2013], forest greenness [*Trujillo et al.,* 2012], growth rates of high-elevation tree species [*Salzer et al.,* 2009], and annual patterns of carbon and nitrogen cycling [*Brooks et al.,* 2011].

Tools for estimating snow accumulation and melt operate at different spatial and temporal scales. Small-scale models, which retain the detailed physics of the energy balance, are useful for evaluating how changes in local-scale energy budgets affect snowpack dynamics. For example, *Kumar et al.* [2012] used the SNOBAL model [*Marks et al.,* 1998] to locally demonstrate how less frequent but more intense storm events could increase the maximum seasonal SWE. Coarser, large-scale energy balance approaches have been used to evaluate temporal trends in SWE for the western U.S. [*Mote et al.,* 2005]. Remote sensing observations (satellite and airborne lidar) of snow cover depth and extent, coupled with in situ measurement of snow density offer improvements for estimating SWE over tens to hundreds of square kilometers [*Barrett*, 2003; *Girotto et al.,* 2014; *Harpold et al.,* 2014; *Kirchner et al.,* 2014; *Rice et al.,* 2011].

Field studies, remote sensing, and modeling efforts all demonstrate that snow depth and water equivalent typically increase with elevation [e.g., *Abatzoglou*, 2011; *Bradley et al.,* 2009; *Clark et al.,* 2011; *Ford et al.,* 2013; *Girotto et al.,* 2014; *Kirchner et al.,* 2014; *Rice et al.,* 2011]. Given this consistent relationship between SWE and elevation, and the expectation of global warming in the range of 1.7 to 4.8°C by 2081–2100 [*Intergovernmental Panel on Climate Change*, 2014], we argue that a watershed's elevation distribution should strongly influence its

©2015. American Geophysical Union. All Rights Reserved.

response to warming-driven snowpack loss. Because catchments draining mountainous terrain exhibit a wide variety of elevation distributions, we expect that snowpack losses will vary from catchment to catchment, generating a complex pattern at the landscape scale.

Here we present a theoretical framework and simulation results designed to quantify the elevation-based sensitivity of mountain watersheds to warming-driven snowpack loss. We identify the metrics important in characterizing a watershed's elevation-based susceptibility to snowpack loss and link our simulation results to landscape sensitivities.

2. Methods and Experimental Design

2.1. Elevation-Based Framework

2.1.1. Elevation Characteristics of Northern Rocky Mountain Watersheds

We characterized the elevation distributions of 3175 mountain watersheds in the U.S. northern Rocky Mountains (Figure S1 in the supporting information), a region covering large portions of central Idaho and western Montana and Wyoming. Variations in the lithology and the tectonic and geomorphic histories of the area produce a diverse set of watershed elevation distributions ideal for testing the sensitivity of mountain catchments to snowpack loss. The characterized watersheds range in size from 18 km^2 to 850 km^2, with a mean area of 86 km^2 and a mean elevation of 1900 m. We used 30 m resolution data from the National Elevation Dataset [*Gesch et al.,* 2002] for our elevation-based analyses.

Several common probability distributions were fit to the northern Rocky Mountain elevation distributions. The goodness of fit for each distribution was determined using the Bayesian Information Criterion [*Claeskens and Hjort*, 2008]. More than 88% (2804) of the surveyed elevation distributions were best described by the generalized extreme value (GEV) distribution [*Kotz and Nadarajah*, 2000]. The GEV distribution is convenient because its probability density function (PDF, equation (1)) can be used to model a variety of distribution types.

$$f(x|k,\mu,\sigma) = \begin{cases} \left(\frac{1}{\sigma}\right)\exp\left(-\left(1+k\frac{(x-\mu)}{\sigma}\right)^{-\frac{1}{k}}\right)\left(\left(1+k\left(\frac{x-\mu}{\sigma}\right)\right)^{-1-\frac{1}{k}}\right), k\neq 0 \\ \left(\frac{1}{\sigma}\right)\exp\left(-\exp\left(-\frac{(x-\mu)}{\sigma}\right)-\left(\frac{(x-\mu)}{\sigma}\right)\right), k=0 \end{cases} \quad (1)$$

In the context of this study, the location parameter (μ) determines the elevation where the distribution is centered (Figure 1a); similar metrics of location include the mean, median, or mode. The scale parameter (σ) determines the variability in the distribution by "compacting" or "stretching" it (Figure 1b); similar metrics for scale include variance or standard deviation. The shape parameter (k) describes the asymmetry and tail behavior of the distribution and is analogous to descriptors such as skewness and kurtosis (Figure 1c). For the natural watershed elevation distributions, no correlation was observed between the GEV parameters location and scale or location and shape (Figure S2) or between any of the GEV parameters and watershed drainage area (Figure S3). A correlation was observed between the scale and shape parameters; a regression was developed (Figure S4) and used in the simulation of elevation distributions.

2.1.2. Monte Carlo Simulation of Mountain Watershed Elevation Distributions

Monte Carlo methods were used to simulate 20,000 elevation distributions that cover a wide range of potential watershed elevation distribution types. The distributions were randomly generated using the GEV PDF (equation (1)) for a given set of location, scale, and shape parameters selected at random from values observed in the U.S. northern Rocky Mountains. Because shape and scale are correlated in natural watersheds (Figure S4), we maintained the observed covariance structure by selecting a shape parameter for each randomly drawn scale parameter in the regression equation (Figure S4). The shape-scale correlation of simulated elevation distributions ($r = -0.566$) closely matched that of real-world elevation distributions ($r = -0.574$).

Using a Monte Carlo approach and the GEV distribution to generate synthetic watershed elevation distributions is advantageous for several reasons. First, the synthetic distributions reflect the characteristics of the natural landscape but overcome potential spatial autocorrelation issues. Second, our simulated

©2015. American Geophysical Union. All Rights Reserved.

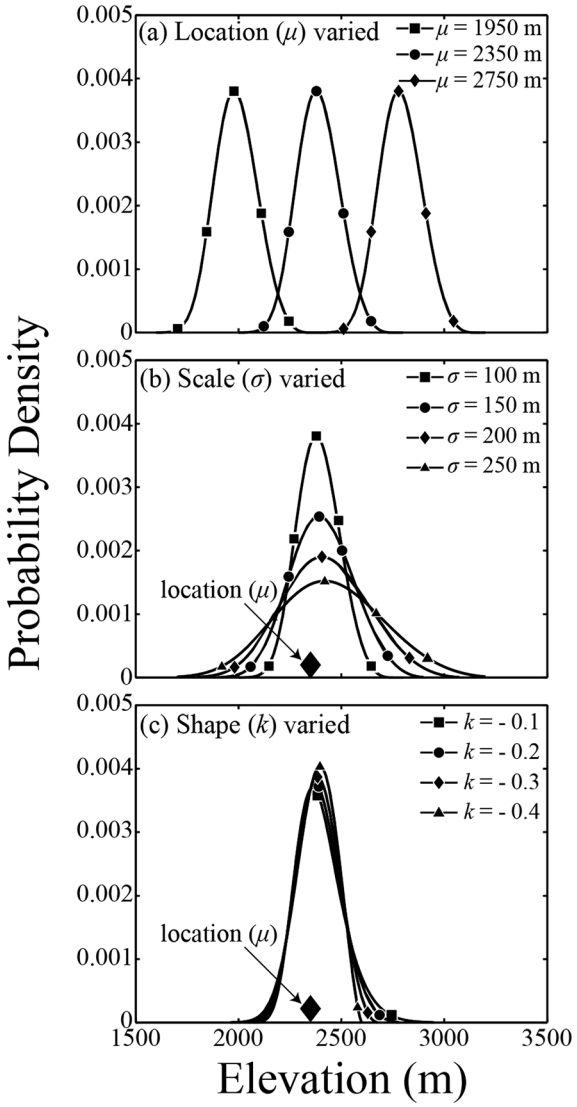

Figure 1. Examples of the influence of (a) location (μ), (b) scale (σ), and (c) shape (k) parameters on a series of generalized extreme value probability distributions for watershed elevations. In each plot, only the labeled variable is changed. The diamonds positioned on the x axis in Figures 1b and 1c show the value of the location parameter for all distributions.

distributions filled in gaps in our sample of natural watersheds, allowing us to explore elevation distributions not common in our sample from the U.S. northern Rocky Mountains. Third, the GEV distribution is defined by three parameters and provides a parsimonious system for distinguishing different distribution types.

2.2. Current and Future Peak SWE-Elevation Relationship

2.2.1. Peak SWE-Elevation Relationship

The peak SWE-elevation relationship defines how average annual peak SWE varies with elevation. We chose peak SWE as a metric of focus because it represents the maximum water accumulation in a snowpack on an annual basis and is important for understanding current snow storage patterns and predicting future ones. We used 1 km^2 gridded estimates of SWE from the National Weather Service's Snow Data Assimilation System (SNODAS) [*Barrett*, 2003; *Carroll et al.*, 2003], a national-scale snow mass and energy model based on SNTHERM.89 [*Jordan*, 1991], to estimate the average peak SWE-elevation relationship for water years 2004–2012. A raster of peak SWE was matched to elevation grids of the same resolution, enabling the calculation of mean peak SWE for each elevation. Although the 2004–2012 water years represent a relatively short time period, they capture a wide range of climatic variability. The 1 April SWE during the 2004–2012 water years ranged from 50 to 130% of the 1981–2010 median 1 April SWE based on SNOTEL records located in the same region. Thus, the SNODAS records represent a range of potential snowpack conditions. However, the number of SNODAS pixels at the highest elevations (>3800 m) within the region of our SWE-based analysis is limited and may not be representative.

We focused on a 36,000 km^2 subregion central to the overall study area to estimate the peak SWE-elevation relationship (Figure S1). The selected region covers a wide range of climate types from maritime influenced to drier continental areas and broadly represents the region of our elevation-based analyses. We evaluated the peak SWE-elevation relationship for other regions within the U.S. northern Rocky Mountains and found that the overall patterns were broadly consistent; peak SWE-elevation relationships have a sigmoidal shape. For all of the surveyed subregions, peak SWE was smallest at low elevations. Near ~1000 m, peak SWE increased rapidly, and at higher elevations, the rate of increase of peak SWE was near zero. While these basic patterns were consistent across the region, maximum peak SWE values and maximum rates of

©2015. American Geophysical Union. All Rights Reserved.

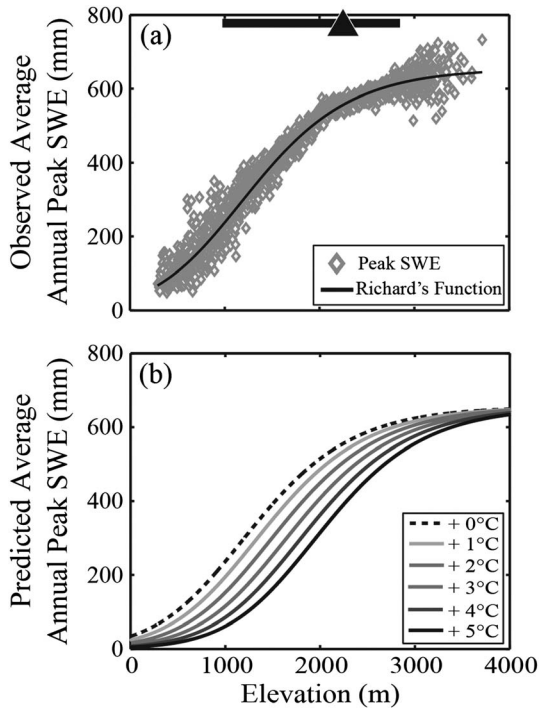

Figure 2. (a) Peak snow water equivalent (SWE) as a function of elevation with the best fit Richard's function (thin black line). Grey diamonds are data from the Snow Data Assimilation System for the region of peak SWE characterization (Figure S1), the thick horizontal line in Figure 2a shows the range of elevations (990–2776 m) where evergreen forest is the dominant land cover type, and the triangle shows the midpoint (2240 m) of the elevation bin where evergreen forests reach their maximum percent cover. (b) Current (+0°C, dashed black line) and expected future changes (darkening solid lines) to the relationship between peak SWE and elevation.

increase in peak SWE can vary with location. The sigmoidal function presented below should be calibrated using local peak SWE-elevation relationships when exact estimates of SWE loss are needed. Because our focus is on developing an elevation-based framework, we chose to use a peak SWE-elevation relationship from a subregion that is broadly representative of the larger region (Figure S1).

2.2.2. Modeling the Current Peak SWE-Elevation Relationship

We used the Richard's growth function, a sigmoidal function, to empirically describe the relationship between peak SWE and elevation (Figure 2a) and to predict future warming-driven modifications (Figure 2b). Peak snow water equivalent (SWE_{pk}) for a given elevation, $elev_i$ (where i ranges from the minimum to maximum elevation) is described using equation (2):

$$SWE_{pk}(elev_i) = A\left[1 + v\ \exp\left\{1 + v + \frac{M}{A}(1+v)^{1+\frac{1}{v}}(\lambda - elev_i)\right\}\right]^{-1/v} \quad (2)$$

where A sets the maximum peak SWE, M is the maximum slope of the curve, λ is a location parameter, and v influences the shape of the function (the location and shape parameters for equation (2) are not related to the location and shape parameter for the GEV PDF, equation (1)). The empirically derived parameters of the Richards equation are convenient because they set a maximum peak SWE value (A) and curve slope (M). The location parameter (λ) can be used to assess the elevation at which SWE exhibits the most rapid increase. These parameters can easily be adjusted to model different observed relationships between peak SWE and elevation and could be used to compare peak SWE-elevation relationships across different mountain regions.

2.2.3. Modeling Potential Future Peak SWE-Elevation Relationships

To model how warming could affect peak SWE, we applied a typical lapse rate of −0.65°C per 100 m to shift the location parameter (λ) in equation (2). Shifting λ raises the elevation zone where rapid increases in peak SWE occur, reduces peak SWE in a systematic manner across all elevations, and is analogous to a warming-driven increase in the elevation of the snowline (Figure 2b). The greatest SWE reductions occur at low and middle elevations where temperatures would more frequently be above 0°C. Increases in precipitation at high elevations may partially offset the impacts of warming [*Girotto et al.,* 2014; *López-Moreno et al.,* 2013]. Our method for modeling the peak SWE-elevation relationship can be modified for anticipated changes in precipitation by modifying parameter A in equation (2) and is flexible enough to accommodate a variety of warming and elevation-dependent changes to the peak SWE-elevation relationship.

2.3. Areal-Average Peak SWE Estimation for Simulated Elevation Distributions

Areal-average peak *SWE* for each of the 20,000 simulated elevation distributions was determined using the following formula:

$$SWE = \sum_{i=1}^{I} SWE_{(i)}(a_i) \quad (3)$$

©2015. American Geophysical Union. All Rights Reserved.

where SWE_i is the peak SWE value at elevation i and a_i is the fraction of total watershed area at elevation i (i ranges from the minimum to maximum watershed elevation (I)). SWE_i for each fraction of area (a_i) was determined using equation (2). Equation (3) was used for determining the current and potential future watershed areal-average peak *SWE* as described in section 2.6.

2.4. Current and Future Snowline Elevations

In landscapes experiencing seasonal snow cover, it is useful to evaluate the duration of snow cover as a function of elevation to understand elevation-dependent streamflow patterns [*Tennant et al.,* 2015], wintertime biogeochemical fluxes [*Brooks et al.,* 2011], and ecological sensitivities of mountain communities [*Bales et al.,* 2006]. Closely linked to the duration of snow cover is the idea of a snowline elevation, which can be useful for characterizing catchment sensitivity to warming-driven hydrologic change. However, a robust definition of the snowline is difficult because of short-term (storm-driven) and long-term (interannual climate-driven) variability in the freezing elevation. Here we define the snowline as the elevation where there is a 50% probability of encountering SWE >0 on an annual basis; elevations above this value would, on average, have snow cover at least 6 months of each year. This snowline definition has precedence [*Hantel and Maurer*, 2011] and designates elevations that have consistent wintertime snow cover from those that do not; other snowline definitions may be appropriate for different sensitivity assessments. We identified the average snowline elevation for water years 2004–2012 by calculating the probability of SWE >0 for all elevations using SNODAS SWE and elevation grids of the same resolution. For the region of climatic characterization (Figure S1), the current snowline elevation is ~1980 m. Shifting the snowline upward using a typical lapse rate results in future snowline elevations of 2134, 2288, 2442, 2595, and 2749 m (for +1°C, 2°C, 3°C, 4°C, and 5°C, respectively).

2.5. Extent of Evergreen Forest

To link our rising snowline and snowpack loss simulations (section 2.2) to a landscape sensitivity, we defined the lower and upper extents of evergreen forest within the region of our peak SWE-elevation characterization. We focused on evergreen forests because of their sensitivity to changes in temperature and water availability [*Salzer et al.,* 2009; *Trujillo et al.,* 2012] and their importance to the hydrologic cycle [*Goulden and Bales*, 2014]. The lower and upper extents of evergreen forest were identified using 30 m resolution elevation data and land cover data from the 2011 National Landcover Database (NLD) [*Jin et al.*, 2013]. We binned the elevations within the region used for climatic characterization (Figure S1) into 10 bins. The corresponding NLD cells that fell within each elevation bin were extracted and used to calculate the percentage that each land cover type composes within each respective elevation bin (Figure S5). The extent of evergreen forest is defined by the elevations of the lower and upper bins where evergreen forest composed the greatest percentage of land cover (Table S1). We evaluated a variety of bin sizes and found that increasing the number of bins had minimal effect on the elevations where evergreen forest was identified as the dominant land cover type.

2.6. Snowpack Sensitivity Metrics

To evaluate the sensitivity of the simulated watershed elevation distributions to warming-driven snowpack loss, we recalculated watershed areal-average peak SWE for a range of increased temperatures (+1°C to +5°C) using equations (2) and (3). Parameters in equation (2) were adjusted for each warming scenario as described above (section 2.2.3 and Figure 2b). Peak SWE loss for a given catchment was determined by differencing the current (+0°C) areal-average peak SWE from a modeled future value (e.g., +5°C). Calculating the area above the snowline (AAS) reveals the percentage of the watershed that maintains snow cover for at least 6 months. We calculated the percent loss in AAS for each warming increment. We report percent loss instead of area loss because the drainage areas of all the simulated elevation distributions are held constant (section 2.1.2).

3. Discussion of Simulation Results

3.1. Peak SWE Loss

Peak SWE losses are controlled by the location and scale parameters of the GEV elevation distributions. The pattern of peak SWE loss is nonlinear across the simulated elevation distributions and forms a parabolic pattern with respect to the location parameter (Figure 3a). The location parameter is the primary control on peak SWE loss while the scale parameter is a lesser, though consistent indicator of peak SWE loss. The greatest

©2015. American Geophysical Union. All Rights Reserved.

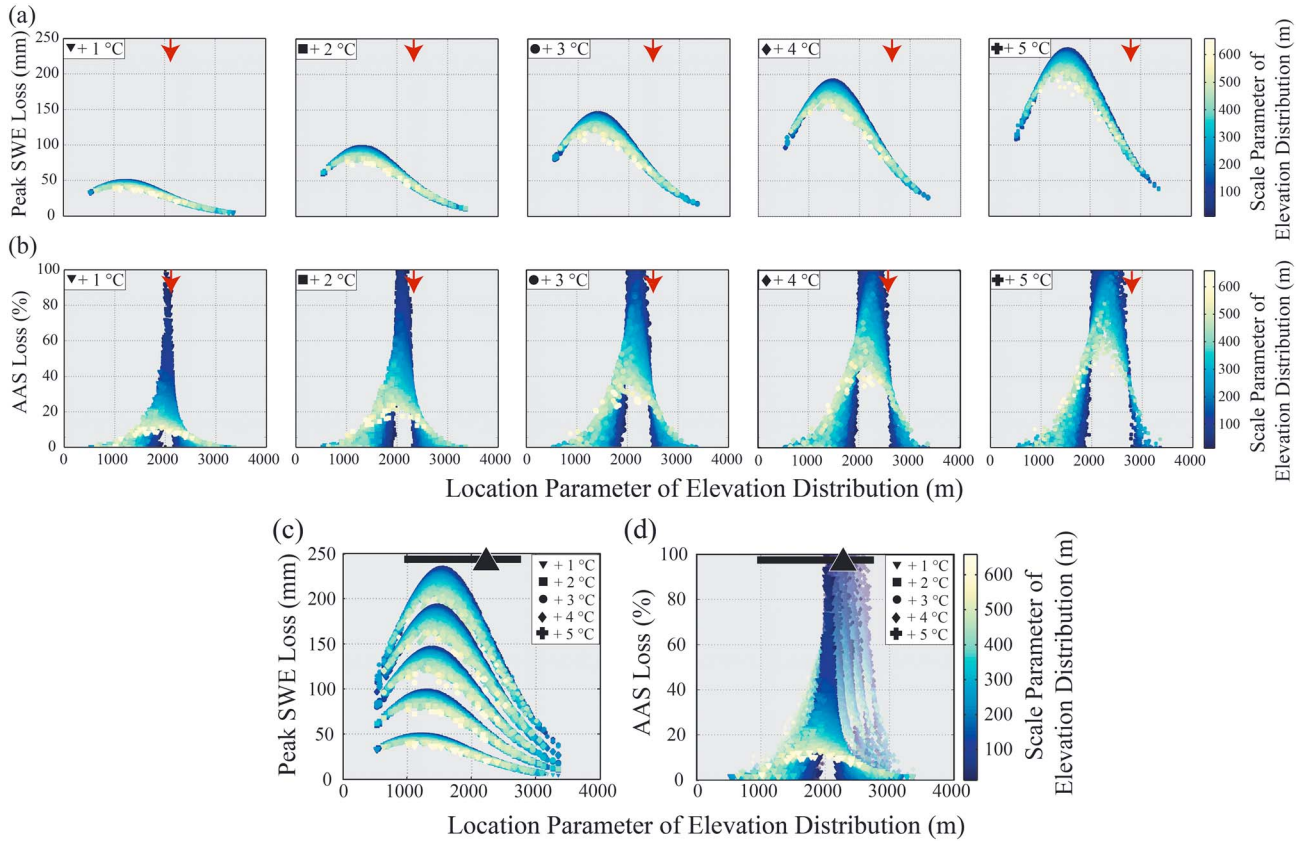

Figure 3. Catchment-wide predictions of (a and c) peak SWE loss and (b and d) loss of area above snowline (AAS) given +1°C to +5°C warming. Each point represents a Monte Carlo-simulated watershed elevation distribution, the location parameter (μ) describes the central tendency and the scale parameter (σ) the variance of the individual distributions. The arrows in Figures 3a and 3b indicate the snowline elevation for each degree of warming. Simulations emphasize that catchment sensitivity varies with peak SWE loss or AAS loss and depends on the location (μ) and scale (σ) parameters of each elevation distribution and the degree of warming. Horizontal bars in Figures 3c and 3d denote the range of elevations (990–2776 m) where evergreen forests are currently the dominant land cover, and the triangles show the midpoint (2240 m) of the elevation bin where evergreen forests reach their maximum percent cover.

losses occur in watersheds with location parameters between 1000 and 2000 m and with scale parameters less than ~300 m. Elevation distributions with higher scale parameters have lower SWE losses even if they are located between 1000 and 2000 m (Figure 3a). The role of large scale parameters in reducing peak SWE loss becomes increasingly apparent as warming progresses (Figure 3a, +5°C). For example, at +5°C warming, elevation distributions with scale parameters ≥600 m have nearly 70 mm less peak SWE loss than watersheds with narrow-elevation distributions. These simulation results demonstrate that only watersheds with location parameters >2000 m and a small number of watersheds located between 1000 and 2000 m with large-scale parameters (≥500 m) are resilient to significant warming. These catchments will serve as persistent water resources and be the most capable of sustaining ecosystems which depend on snow-dominated hydrology.

We performed multivariate regression analysis to quantify how elevation distributions influence the patterns of peak SWE loss (Table S1). For +1°C to +5°C, we used the Bayesian Information Criterion (BIC) to select the most parsimonious regression from all model subsets of the GEV parameters up to third-order GEV interactions (e.g., location^3 or location × shape^2; all regressions had $R^2 = 0.99$). The GEV elevation parameters that explained the most variance in peak SWE loss were location and scale. Of these regression parameters, location^2 explained the majority of the variance in peak SWE loss across all warming scenarios. The variance explained by location^2 and location^3 increases with warming (Figure S6) and emphasizes the highly nonlinear, elevation-dependent response of peak SWE loss (Figure 3a). The GEV shape parameter was selected in each regression by BIC (Table S2), however, it explained <0.5% of the variance in peak SWE loss across all warming scenarios.

©2015. American Geophysical Union. All Rights Reserved.

The peak SWE loss results presented here demonstrate that multiparameter descriptions of elevation distributions will prove useful in estimating catchment sensitivity to snowpack loss. Our simulation results are consistent with *Pederson et al.* [2013] and *Stewart* [2009], showing that middle elevations are the most sensitive to warming-driven snowpack loss. We add to these results by demonstrating and quantifying the potential nonlinear, elevation-dependent response of mountain catchments to SWE loss (Figure 3a).

3.2. Area Above Snowline Loss

Patterns of area above snowline (AAS) loss are strongly influenced by the location of an elevation distribution relative to the elevation of the snowline. The greatest losses occur for watersheds centered just below the snowline elevation (Figure 3b). The scale parameter also plays an important role in regulating AAS loss. For example, in the +1°C warming scenario, AAS loss for elevation distributions centered just below the snowline can be as great as 100% for those with small variance in elevation (scale $<$200 m), whereas those with larger variance (scale $>$500 m) experience AAS loss of less than 10%.

Warming causes the patterns of AAS loss to shift in complex ways. For example, the elevation zone where the greatest AAS losses are focused expands with warmer temperatures and the value of minimum AAS loss within this zone increases (Figure 3c). At +5°C, only a small number of watershed elevation distributions have not experienced significant AAS loss. These catchments have location parameters greater than ~2800 m and scale parameters less than 300 m. These AAS loss simulations reinforce that multiparameter descriptions of elevation distributions are crucial to characterizing catchment sensitivity to snowpack loss.

3.3. Potential Model Limitations

We expect our elevation-based framework to be widely applicable, but it may be ill suited for some locations or situations. The GEV PDF produces distributions that tend to be smoother than natural ones. Thus, catchments with strong asymmetry or bimodality in their elevation distributions may not be as well represented.

The peak SWE-elevation relationship used in our simulations involved large-scale spatial averaging, collapsing the many nonuniform physical processes (e.g., sublimation, wind redistribution, ablation, and avalanching) controlling the spatial distribution of SWE into a single, elevation-dependent metric. A central assumption is that the processes controlling the energy and mass balance over the years that are summarized by the peak SWE-elevation relationship can be shifted to represent future ones (e.g., Figure 2b). Because our framework is centered on fundamental principles like temperature lapse rate and orographic precipitation enhancement (see review in *Roe* [2005]), we assert that it provides adequate first-order estimates of watershed sensitivity to snowpack loss.

Our framework is intended to be applied at the intermediate watershed scale (50 km^2 to 1000 km^2) because SWE amounts at these scales are dominantly influenced by the freezing level elevation, snowfall amounts, and available melt energy [*Abatzoglou*, 2011; *Bradley et al.,* 2009; *Clark et al.,* 2011; *Elder et al.,* 1998]. Variations in SWE at the hillslope to small-catchment (~0.5 to 10 km^2) scales caused by drifting [*Luce et al.,* 1998], interception by vegetation [*Varhola et al.,* 2010], sublimation [*Gustafson et al.,* 2010], and avalanching [*Clark et al.,* 2011] are lumped in our functional relationship between peak SWE and elevation (Figure 2). Although these processes may govern SWE variability at smaller scales or when relief is less than ~200 m [*Clark et al.,* 2011], we expect that at intermediate watershed scales and above, the model will perform well.

The results from our simulations are theoretical, and an important future step is to evaluate how well this characterization matches observed snowpack loss on the landscape. To rigorously evaluate our framework, long-term estimates of peak SWE that span large-elevation gradients from a number of different catchments having experienced a warming trend are needed. Lidar snow-on, snow-off depth estimates [*Harpold et al.,* 2014] coupled with spatially extensive density measurements may soon provide data sets that allow a rigorous test of our framework.

3.4. Examples of Model Application

3.4.1. Watershed Sensitivity Analyses

Our results indicate that catchment sensitivity to warming depends on the elevation distribution of a watershed and which consequences are of greatest concern. For example, following +5°C of warming, the greatest peak SWE losses occur in watersheds centered at 1500 m; however, the greatest AAS losses occur around 2250 m. Therefore, catchment sensitivity needs to be clearly defined for particular management

©2015. American Geophysical Union. All Rights Reserved.

needs or research questions. The framework and regression models presented here could be used to estimate the amount of peak SWE or AAS loss for a given amount of warming to identify which watersheds are most capable of sustaining snow-based water resources. Our framework is easily applied to categorize sensitive versus resilient watersheds or to prioritize the rehabilitation of habitat for snowmelt-dependent aquatic species. Our snowpack loss simulations offer a probability space of potential watershed responses to warming and could be used to focus the efforts of physically based models to identify mechanistic controls on watersheds that are expected to be either sensitive or resilient to warming.

3.4.2. Sensitivity of Evergreen Forests to Peak SWE and AAS Loss

We found that evergreen forests are the dominant land cover type within the sensitive middle elevations (1000–2000 m; Figure S5). Furthermore, the peak areal extent of evergreen forest cover was located between 2000 and 2400 m (Table S1); our AAS and peak SWE loss simulations (Figures 3c and 3d) indicate that these elevations will likely experience decreases in snow cover amount and duration. *Trujillo et al.* [2012] report that forest greenness, an indicator of forest health, is strongly correlated with peak SWE, and predict that middle-elevation mountain forests are highly sensitive to temperature increases. Our results confirm that middle elevations are highly sensitive to peak SWE loss but show that different watershed elevation distributions will likely exhibit different peak SWE losses, even if the mean catchment elevation (location) is held constant. Thus, some forested basins may be more sensitive or more resilient than expected if sensitivity were evaluated on their mean elevations alone. Further, because snow cover duration influences wintertime heterotrophic activity [*Brooks et al.,* 2011], our AAS loss model could improve predictions of which catchments are most likely to experience decreased carbon (C) and nitrogen (N) cycling occurring during winter months (Figure 3d).

4. Conclusions

The expectation of future warming and strong anthropogenic and ecosystem ties to melt-supplied water sources drive the need to map the potential trajectories of snowpack loss in sensitive mountain catchments. The framework presented here provides a parsimonious method for characterizing the potential sensitivity of individual mountain catchments to snowpack loss.

Acknowledgments

The elevation data used for this paper are available from the National Elevation Dataset (http://ned.usgs.gov/). The Snow Data Assimilation System (SNODAS) snow water equivalent (SWE) data can be obtained at the National Snow and Ice Data Center's Polaris tool (http://nsidc.org/data/polaris/). All MATLAB and *R* scripts used in the presented analyses are available upon request from the lead author. The work was supported by a NASA Idaho Space Grant Consortium Fellowship and by NSF awards EPS-0814387 and EPS-1006968 from the Idaho NSF EPSCoR Program. This work benefited from conversations and feedback from Noah Molotch, Paul Brooks, Kathleen Lohse, John Welhan. We thank Keith Musselman and an anonymous reviewer.

The Editor thanks Keith Musselman and an anonymous reviewer for their assistance in evaluating this paper.

References

Abatzoglou, J. T. (2011), Influence of the PNA on declining mountain snowpack in the western United States, *Int. J. Climatol.*, *31*, 1135–1142, doi:10.1002/joc.2137.

Bales, R. C., N. P. Molotch, T. H. Painter, M. D. Dettinger, R. Rice, and J. Dozier (2006), Mountain hydrology of the western United States, *Water Resour. Res.*, *42*, W08432, doi:10.1029/2005WR004387.

Barrett, A. P. (2003), National operational hydrologic remote sensing center snow data assimilation system (SNODAS) products at NSIDC, in *NSIDC Spec. Rep*, vol. 11, pp. 19, Natl. Snow and Ice Data Cent., Boulder, Colo.

Bradley, R. S., F. T. Keimig, H. F. Diaz, and D. R. Hardy (2009), Recent changes in freezing level heights in the Tropics with implications for the deglacierization of high mountain regions, *Geophys. Res. Lett.*, *36*, L17701, doi:10.1029/2009GL037712.

Brooks, P. D., P. Grogan, P. H. Templer, P. Groffman, M. G. Öquist, and J. Schimel (2011), Carbon and nitrogen cycling in snow-covered environments, *Geogr. Compass*, *5*(9), 682–699, doi:10.1111/j.1749-8198.2011.00420.x.

Carroll, T., D. Cline, G. Fall, L. Li, and A. Nilsson (2003), Seasonal snow cover monitoring and modeling for the coterminous United States, paper presented at EGS-AGU-EUG Joint Assembly, Nice, France, 1396.

Claeskens, G., and N. L. Hjort (2008), *Model Selection and Model Averaging (Cambridge Series in Statistical and Probabilistic Mathematics)*, Cambridge Univ. Press, Cambridge, New York.

Clark, G. M. (2010), Changes in patterns of streamflow from unregulated watersheds in Idaho, Western Wyoming, and Northern Nevada, *J. Am. Water Resour. Assoc.*, *46*(3), 486–497, doi:10.1111/j.1752-1688.2009.00416.x.

Clark, M. P., J. Hendrikx, A. G. Slater, D. Kavetski, B. Anderson, N. J. Cullen, T. Kerr, E. O. Hreinsson, and R. A. Woods (2011), Representing spatial variability of snow water equivalent in hydrologic and land-surface models: A review, *Water Resour. Res.*, *47*, W07539, doi:10.1029/2011WR010745.

Elder, K., W. Rosenthal, and R. E. Davis (1998), Estimating the spatial distribution of snow water equivalence in a montane watershed, *Hydrol. Processes*, *12*(10–11), 1793–1808, doi:10.1002/(SICI)1099-1085(199808/09)12:10/11<1793::AID-HYP695>3.0.CO;2-K.

Ford, K. R., A. K. Ettinger, J. D. Lundquist, M. S. Raleigh, and J. H. R. Lambers (2013), Spatial heterogeneity in ecologically important climate variables at coarse and fine scales in a high-snow mountain landscape, *Plos One*, *8*(6), e65008, doi:10.1371/journal.pone.0065008.

Gesch, D., M. Oimoen, S. Greenlee, C. Nelson, M. Steuck, and D. Tyler (2002), The national elevation dataset, *Photogramm. Eng. Remote Sens.*, *68*(1), 5–32.

Girotto, M., G. Cortes, S. A. Margulis, and M. Durand (2014), Examining spatial and temporal variability in snow water equivalent using a 27 year reanalysis: Kern River watershed, Sierra Nevada, *Water Resour. Res.*, *50*, 6713–6734, doi:10.1002/2014WR015346.

Goulden, M. L., and R. C. Bales (2014), Mountain runoff vulnerability to increased evapotranspiration with vegetation expansion, *Proc. Natl. Acad. Sci. U.S.A.*, *111*(39), 14,071–14,075, doi:10.1073/pnas.1319316111.

Gustafson, J. R., P. D. Brooks, N. P. Molotch, and W. C. Veatch (2010), Estimating snow sublimation using natural chemical and isotopic tracers across a gradient of solar radiation, *Water Resour. Res.*, *46*, W12511, doi:10.1029/2009WR009060.

Hantel, M., and C. Maurer (2011), The median winter snowline in the Alps, *Meteorol. Z.*, *20*(3), 267–276, doi:10.1127/0941-2948/2011/0495.

©2015. American Geophysical Union. All Rights Reserved.

Harpold, A. A., et al. (2014), LiDAR-derived snowpack data sets from mixed conifer forests across the Western United States, *Water Resour. Res.*, *50*(3), 2749–2755, doi:10.1002/2013WR013935.

Intergovernmental Panel on Climate Change (2014), Summary for Policymakers, in *Climate Change 2014: Impacts, Adaptation, and Vulnerability. Part A: Global and Sectoral Aspects. Contribution of Working Group II to the Fifth Assessment Report of the Intergovernmental Panel on Climate Change*, edited by C. B. Field et al., pp. 1–32, Cambridge Univ. Press, Cambridge, U. K., and New York.

Jin, S., L. Yang, P. Danielson, C. Homer, J. Fry, and G. Xian (2013), A comprehensive change detection method for updating the National Land Cover Database to circa 2011, *Remote Sens. Environ.*, *132*, 159–175.

Jordan, R. (1991), A one-dimensional temperature model for a snow cover: Technical documentation for SNTHERM. 89, U.S. Army Cold Regions Research and Engineering Laboratory Special Rep., 91–16, pp. 1–49 .

Kirchner, P., R. Bales, N. Molotch, J. Flanagan, and Q. Guo (2014), LiDAR measurement of seasonal snow accumulation along an elevation gradient in the southern Sierra Nevada, California, *Hydrol Earth Syst. Sci. Disc.*, *18*(10), 4261–4275, doi:10.5194/hess-18-4261-2014.

Knowles, N., M. D. Dettinger, and D. R. Cayan (2006), Trends in snowfall versus rainfall in the Western United States, *J. Clim.*, *19*(18), 4545–4559, doi:10.1175/jcli3850.1.

Kotz, S., and S. Nadarajah (2000), *Extreme Value Distributions*, Imperial College Press, London.

Kumar, M., R. Wang, and T. E. Link (2012), Effects of more extreme precipitation regimes on maximum seasonal snow water equivalent, *Geophys. Res. Lett.*, *39*, L20504, doi:10.1029/2012GL052972.

López-Moreno, J. I., J. W. Pomeroy, J. Revuelto, and S. M. Vicente-Serrano (2013), Response of snow processes to climate change: Spatial variability in a small basin in the Spanish Pyrenees, *Hydrol. Processes*, *27*(18), 2637–2650, doi:10.1002/hyp.9408.

Luce, C. H., D. G. Tarboton, and R. R. Cooley (1998), The influence of the spatial distribution of snow on basin-averaged snowmelt, *Hydrol. Processes*, *12*(10–11), 1671–1683, doi:10.1002/(sici)1099-1085(199808/09)12:10/11<1671::aid-hyp688>3.0.co;2-n.

Marks, D., J. Kimball, D. Tingey, and T. Link (1998), The sensitivity of snowmelt processes to climate conditions and forest cover during rain-on-snow: A case study of the 1996 Pacific Northwest flood, *Hydrol. Processes*, *12*(10–11), 1569–1587, doi:10.1002/(sici)1099-1085(199808/09)12:10/11<1569::aid-hyp682>3.3.co;2-c.

Mote, P. W., A. F. Hamlet, M. P. Clark, and D. P. Lettenmaier (2005), Declining mountain snowpack in western North America, *Bull. Am. Meteorol. Soc.*, *86*(1), 39–49, doi:10.1175/bams-86-1-39.

Pederson, G. T., J. L. Betancourt, and G. J. McCabe (2013), Regional patterns and proximal causes of the recent snowpack decline in the Rocky Mountains, US, *Geophys. Res. Lett.*, *40*(9), 1811–1816, doi:10.1002/grl.50424.

Rangwala, I., and J. R. Miller (2012), Climate change in mountains: A review of elevation-dependent warming and its possible causes, *Clim. Change*, *114*(3–4), 527–547, doi:10.1007/s10584-012-0419-3.

Rice, R., R. C. Bales, T. H. Painter, and J. Dozier (2011), Snow water equivalent along elevation gradients in the Merced and Tuolumne River basins of the Sierra Nevada, *Water Resour. Res.*, *47*, W08515, doi:10.1029/2010WR009278.

Roe, G. H. (2005), Orographic precipitation, in *Annual Review of Earth and Planetary Sciences*, edited, pp. 645–671, Annual Reviews, Palo Alto, doi: 10.1146/annurev.earth.33.092203.122541.

Salzer, M. W., M. K. Hughes, A. G. Bunn, and K. F. Kipfmueller (2009), Recent unprecedented tree-ring growth in bristlecone pine at the highest elevations and possible causes, *Proc. Natl. Acad. Sci. U.S.A.*, *106*(48), 20,348–20,353, doi:10.1073/pnas.0903029106.

Stewart, I. T. (2009), Changes in snowpack and snowmelt runoff for key mountain regions, *Hydrol. Processes*, *23*, 78–94, doi:10.1002/hyp.7128.

Tennant, C. J., B. T. Crosby, and S. E. Godsey (2015), Elevation-dependent responses of streamflow to climate warming, *Hydrol. Processes*, *29*, 991–1001, doi:10.1002/hyp.10203.

Trujillo, E., N. P. Molotch, M. L. Goulden, A. E. Kelly, and R. C. Bales (2012), Elevation-dependent influence of snow accumulation on forest greening, *Nat. Geosci.*, *5*(10), 705–709, doi:10.1038/ngeo1571.

Varhola, A., N. C. Coops, M. Weiler, and R. D. Moore (2010), Forest canopy effects on snow accumulation and ablation: An integrative review of empirical results, *J. Hydrol.*, *392*(3–4), 219–233, doi:10.1016/j.jhydrol.2010.08.009.

©2015. American Geophysical Union. All Rights Reserved.